Ultrafast Crystallization of Ordered Mesoporous Metal Oxides and Carbon in Seconds

Leyan Wang,[†] Geok Leng Seah,[†] Yun Li,[†] Wei Han Tu,[†] Edward W. Corcoran Jr.,[‡] Adam K. Usadi,[‡] Jonathan M. McConnachie,[‡] Hock Guan Ong,[⊥] and Kwan W. Tan[†,]*

[†]School of Materials Science and Engineering, Nanyang Technological University, Singapore 639798, Singapore.

[‡]ExxonMobil Research and Engineering Company, Annandale, New Jersey 08801, United States.

[⊥]Smart Memories Pte Ltd, Singapore 048545, Singapore.

[*]Corresponding Author: kwtan@ntu.edu.sg

ABSTRACT

Conventional heat treatments to generate well-ordered and crystalline mesoporous oxide and carbon structures are limited by long durations and annealing temperatures that can cause mesostructural collapse. This Communication describes a facile strategy coupling block copolymer-directed self-assembly with high-power Joule heating to form highly crystalline and long-range ordered mesoporous oxide and carbon nanostructures in just a few seconds. The combined approach is compatible with various self-assembled hybrid systems, generating mesoporous composites of γ-Al_2O_3-carbon, γ-Al_2O_3/MgO-carbon and anatase-TiO_2-carbon with *p*6*mm* symmetry, as well as mesoporous non-close-packed carbon structures. Removing the polymer/carbon gives well-defined mesoporous all-γ-Al_2O_3 and all-anatase-TiO_2 structures. Impregnation of chloroplatinic acid followed by Joule heating yields platinum nanoparticles decorated on the channel walls of mesoporous γ-Al_2O_3-carbon structures. The rapid formation of thermally stable and periodically ordered crystalline oxide, carbon and oxide-carbon structures may be appealing for catalysis, carbon sequestration and energy-related applications.

MAIN TEXT

Highly crystalline, ordered mesoporous oxide and carbon materials generated by structure-directing surfactants and block copolymers (BCPs) are desirable for their tunable periodic morphologies and multifunctional properties,[1–7] and have been widely deployed in many applications[8] ranging from catalysis,[9,10] energy conversion and storage,[11–14] adsorption and separation,[15,16] sensing[17,18] and even superconductors.[19] However, conventional routes to form mesoporous inorganic structures with high crystallinity typically require thermal annealing treatments at elevated temperatures (≥600 °C) over long durations (≥10 hours) under controlled environments (e.g., argon, ammonia) for inorganic crystallization, thereby increasing production time and cost.[3–7,15–19] In particular, untamed nucleation and growth of crystallites that occur spontaneously at higher temperatures often result in the collapse of ordered structures.[2,5,7]

Alternative nonequilibrium methods have been explored for the rapid formation of single crystal and polycrystalline inorganic nanostructures on shorter time frames.[20–29] For example, Tan *et al.* demonstrated an all-laser-induced approach coupling BCP-directed self-assembly of resols with sub-millisecond laser heating (B-WRITE) to write hierarchically mesoporous polymer and carbon thin film structures.[21] Periodically ordered mesoporous crystalline silicon nanostructures were then obtained by filling the continuous network polymer template with amorphous silicon, followed by nanosecond laser-induced melt-crystallization and template removal.[21–23] Microwave annealing of mesoporous metal oxide thin films has been described but it required several minutes attaining limited crystallinity.[25] More recently, Hu *et al.* and Tour *et al.* reported a rapid Joule heating-based method generating discrete high-entropy metal nanoparticles,[26,27] sintered pellets of garnet ceramics with low porosity[28] and turbostratic graphene layers[29] on the milli- to tens of second timescales. We hypothesize

pairing soft matter–directed self-assembly with Joule heating to form highly crystalline, well-ordered mesoporous inorganic structures could open new pathways to access unique functional property profiles, expand parameter and application space, as well as develop new fundamental understanding of processing–structure–property correlations. Shorter heating dwells could enable better control of crystallite growth and prevent agglomeration or mesostructure collapse. To this end, we describe Joule heating of block copolymer-directed hybrid monoliths generating highly crystalline and periodically ordered mesoporous inorganic oxides and carbon within seconds, to the best of our knowledge, for the first time.

The self-assembly and nonequilibrium annealing phase transformation (SNAP) approach is shown in Scheme 1. We employed amphiphilic BCPs of polyethylene oxide-*block*-polypropylene oxide-*block*-polyethylene oxide (F127) and polystyrene-*block*-polyethylene oxide (PS-*b*-PEO) as structure-directors for metal oxide sols and phenol-formaldehyde resols (additives) to form hybrid monoliths with ordered morphologies by evaporation induced self-assembly (EISA). The as-made monoliths were cured to thermopolymerize the BCP into a rigid resin support. The self-assembled composites were then Joule-heated at 70–420 W for 1–100 s under mild vacuum, yielding highly crystalline and periodically ordered mesoporous oxide-carbon and carbon structures. Removal of the polymer/carbon matrix gave access to well-defined crystalline mesoporous oxide structures. Herein, samples are denoted as SNAP-*X*-*Y*-*Z*, where *X* is the additive, *Y* is the rigid support and *Z* is the Joule heating duration.

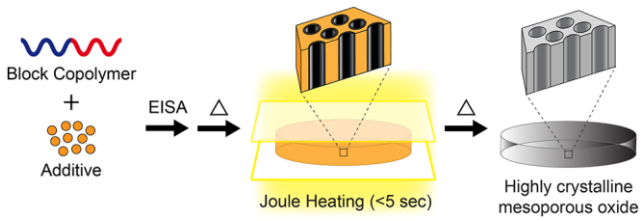

Scheme 1. Schematic of SNAP approach.

Figure 1 shows the structural evolution of F127-directed SNAP-Al_2O_3 mesostructures that were annealed at 360 W for 1 to 100 s using small- and wide-angle X-ray scattering (SAXS/WAXS) and summarized in Table 1. Consistent with our previous study the Al_2O_3-hybrid has a long-range ordered *p*6*mm* lattice with a channel-to-channel *d*-spacing of 20 nm as confirmed by SAXS.[16] However, direct Joule heating of the hybrid resulted in sample pulverization attributed to thermal shock effects and poor thermal stability. To improve structural integrity, as-made samples were cured at 400 °C under N_2 converting the BCP into thermopolymerized resin (Figure S1). SAXS indicates Al_2O_3-resin retained the *p*6*mm* symmetry with a smaller *d*-spacing of 13.4 nm due to thermal shrinkage, while the absence of peaks in WAXS pattern indicates amorphous Al_2O_3-resin composite (Figure 1).[16]

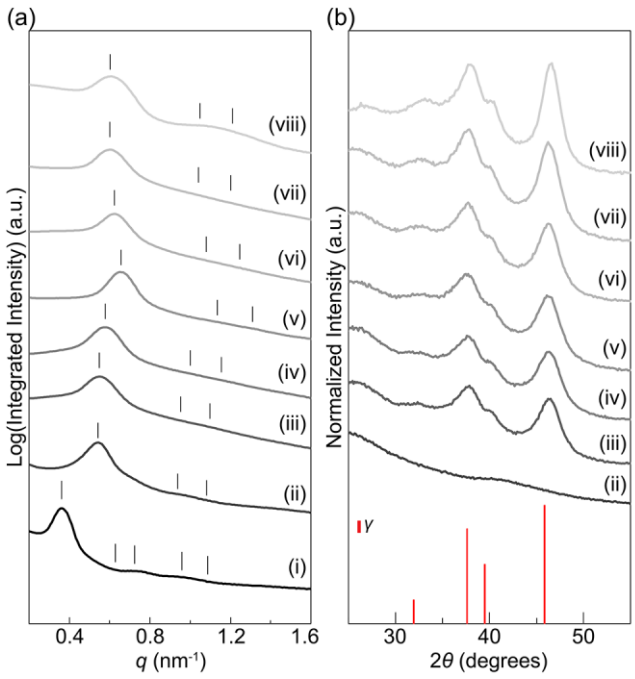

Figure 1. (a) SAXS and (b) WAXS patterns of SNAP-Al_2O_3 samples at different stages: (i) as-made hybrid, (ii) thermal curing, followed by Joule heating at 360 W for (iii) 1, (iv) 5, (v) 25, (vi) 50 and (vii) 100 s. The all-γ-Al_2O_3 (sample (viii)) was generated by calcination at 450 °C, followed by annealing at 360 W for 5 s. Tick marks in (a) indicate expected SAXS

reflections for *p*6*mm* lattice. WAXS peak markings and relative intensities for γ-Al_2O_3 (red, PDF 00-010-0425) are shown in (b)

Table 1. Structural characteristics of SNAP samples.

sample	q*,[a] nm^{-1}	*d*-spacing,[a] nm	morphology[b]	crystallite size,[c] nm	input power
Al_2O_3-hybrid	0.36	20.0	*p*6*mm*		
Al_2O_3-resin	0.54	13.4	*p*6*mm*		
Al_2O_3-C-1s	0.55	13.2	*p*6*mm*	4.4	360 W
Al_2O_3-C-5s	0.58	12.6	*p*6*mm*	4.9	360 W
Al_2O_3-C-25s	0.66	11.1	*p*6*mm*	4.6	360 W
Al_2O_3-C-50s	0.62	11.6	*p*6*mm*	6.1	360 W
Al_2O_3-C-100s	0.60	12.1	*p*6*mm*	6.4	360 W
all-γ-Al_2O_3-5s	0.60	12.0	*p*6*mm*	4.3	360 W
Al_2O_3/MgO-hybrid	0.31	23.5	*p*6*mm*		
Al_2O_3/MgO-resin	0.36	20.2	*p*6*mm*		
Al_2O_3/MgO-C-1s	0.41	17.9	*p*6*mm*		300 W
Al_2O_3/MgO-C-100s	0.51	14.3	*p*6*mm*	5.3	300 W
TiO_2-hybrid	0.16	44.5	*p*6*mm*		
TiO_2-resin	0.19	37.7	*p*6*mm*		
TiO_2-C-1s(70 W)	0.18	39.3	*p*6*mm*	2.0	70 W
TiO_2-C-1s(140 W)	0.19	37.7	*p*6*mm*	2.7	140 W
TiO_2-C-1s(240 W)	0.22	33.3	*p*6*mm*	7.1	240 W
TiO_2-C-1s(320 W)	0.20	35.5	*p*6*mm*	15.2	320 W
TiO_2-C-1s(420 W)	0.21	34.9	*p*6*mm*	17.3	420 W
all-anatase-TiO_2(240 W)	0.22	33.2	*p*6*mm*	7.1	240 W
Carbon-50s	0.19	32.6	non-close-packed micellar	2.8	300 W

[a] Determined by SAXS. [b] Determined by SAXS and TEM. [c] Determined by WAXS.

We then applied nonequilibrium Joule heating on the Al_2O_3-resin monoliths. SAXS (Figure 1a) and transmission electron microscopy (TEM) (Figure 2a) show the γ-Al_2O_3-C composites retained their *p*6*mm* symmetry after annealing at 360 W for 1 to 25 s, accompanied by the decrease of *d*-spacing values by 18% to ~11 nm. Raman spectroscopy indicates the thermopolymerized resin was carbonized by Joule heating (Figure S1b). More remarkably, we observe strong WAXS reflections (Figure 1b) and crystalline fringes in HR-TEM (Figure 2b), affirming crystallization of well-ordered mesoporous γ-Al_2O_3 structures under effective annealing dwell of 1 s. From the Scherrer equation we estimated the average γ-Al_2O_3 crystallite size as 4–5 nm. It is noteworthy to highlight obtaining similar sized crystallites by conventional thermal annealing would require a total of 18 hours for crystallization into γ-

Al_2O_3 at 900 °C,[16] i.e., more than 5 orders of magnitude longer compared to the SNAP duration of <5 s (i.e., including ramp dwell of 3 s).

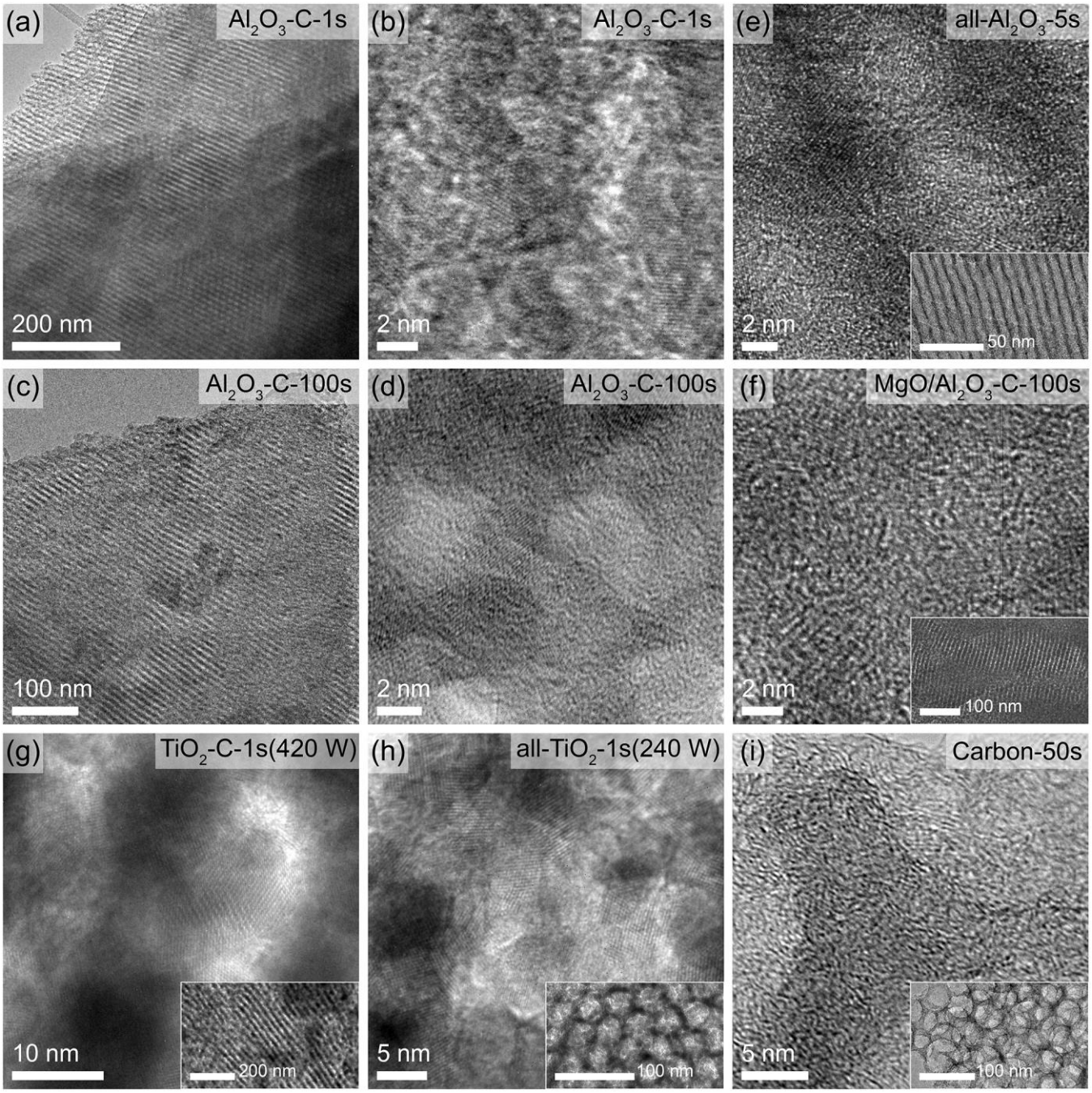

Figure 2. Electron microscopy of SNAP samples. (a, c) TEM and (b, d) HR-TEM of Al_2O_3-C-1s (a, b) and Al_2O_3-C-100s (b,d). (e–i) HR-TEM and TEM (insets) of (e) all-Al_2O_3-5s (f) Al_2O_3/MgO-C-100s, (g) TiO_2-C-1s(420 W), (h) all-TiO_2-1s(240 W) and (i) carbon-50s.

Extending SNAP duration to 50 and 100 s enabled growth of γ-Al_2O_3 crystallites to ~6 nm in Al_2O_3-C whilst retaining the *p*6*mm* periodic order as corroborated by WAXS and SAXS, respectively (Figure 1). In particular, TEM shows the projection of parallel-aligned cylinders and HR-TEM depicts a highly crystalline γ-Al_2O_3 lattice of mesopores after SNAP at 360 W for 100 s (Figure 2c, d). We speculate the BCP-derived carbon acts as a rigid support for Al_2O_3 crystallization, preserving the mesoscale order and macroscale monolithic shape (Figure S2).[5,7,21,22] We further demonstrated the SNAP method facilitates formation of well-defined and crystalline all-oxide structures with *p*6*mm* order. Al_2O_3-hybrid was calcined in air at 450 °C removing BCP and leaving behind amorphous Al_2O_3 structure (Figure S3a).[16] Applying SNAP at 360 W for 5 s induced crystallization of mesoporous all-γ-Al_2O_3 with *p*6*mm* channels of *d*-spacing of 12 nm and a crystallite size of ~4 nm, see SAXS/WAXS of sample (viii) in Figure 1 and TEM/HR-TEM in 2e, as well as Raman spectroscopy in Figure S3d. However, increasing SNAP duration to 100 s resulted in mesostructural collapse due to extensive crystallite growth of α-Al_2O_3 and other Al_2O_3-compounds (Figure S3b, c).

SNAP method is compatible with other multicomponent ordered hybrid systems. For instance, we applied SNAP on mixed Al_2O_3/MgO-resin monoliths at 360 W for 1 and 100 s. Interestingly, no crystallization was observed in Al_2O_3/MgO-C-1s likely due to the Mg atoms inhibiting crystallization of the Al_2O_3 matrix (Figure S4).[7,30] Further increase of SNAP duration to 100 s enabled formation of highly crystalline mesoporous γ-Al_2O_3/MgO–C channels with *p*6*mm* order as corroborated by the SAXS, WAXS and TEM/HR-TEM data displayed in Figure 3a, b and 2f, respectively. Energy dispersive spectroscopy mapping analysis confirmed homogenous Mg distribution in the hexagonal cylinders of mesoporous γ-Al_2O_3/MgO-C-100s (Figure S5).

To better understand processing-structure-property relationships, we applied SNAP method to PS-*b*-PEO–directed hybrid mesostructures with larger lattice constant and pore size. The PS-*b*-PEO-TiO_2-resin composites were cured at 200 °C in a vacuum oven. Figure S6 shows the structural evolution of TiO_2-C composites that were annealed with increasing electrical powers, all for 1 s. WAXS pattern of cured TiO_2-resin hybrid exhibits relatively broad peaks, suggesting a low degree of anatase crystallinity (Figure S6b).[31] Applying Joule heating improved the crystallinity of SNAP-TiO_2 samples significantly. SAXS and TEM verified the larger mesoporous TiO_2-C hexagonal cylinders retained their long-range *p*6*mm* symmetry with *d*-spacing values of 33–39 nm for powers up to 420 W (see Figure 2g, 3a and S6a). The average crystallite size of anatase-TiO_2-C structures first grew from approximately 2 to 7 nm as powers increased from 70, 140 to 240 W, and further increased by twofold to ~17 nm for higher powers of 320 and 420 W (see Figure S6b and HR-TEM in Figure 2g). We note the appearance of new reflections in the WAXS pattern of TiO_2-C-1s(420 W) consistent with crystalline rutile phase, although the sample remained predominantly anatase (Figure 3b). This suggests that ~400 W is the onset power for phase transformation of anatase TiO_2 to rutile in SNAP. To put it another way, higher electrical powers are essential to overcome the activation energy barriers enabling crystalline–crystalline phase transformations for shorter dwells. To obtain mesoporous all-TiO_2 structures, TiO_2-C-1s(240 W) was heated in a static air furnace at 400 °C for 30 min to remove the carbon matrix.[5,7] SAXS and WAXS in Figure S7 and TEM in Figure 2h confirm the white-colored mesoporous all-anatase-TiO_2 monolith retained the *p*6*mm* morphology with similar crystallite size of 7 nm, while the disappearance of D- and G-bands in the Raman spectrum confirms carbon removal (Figure S7e).

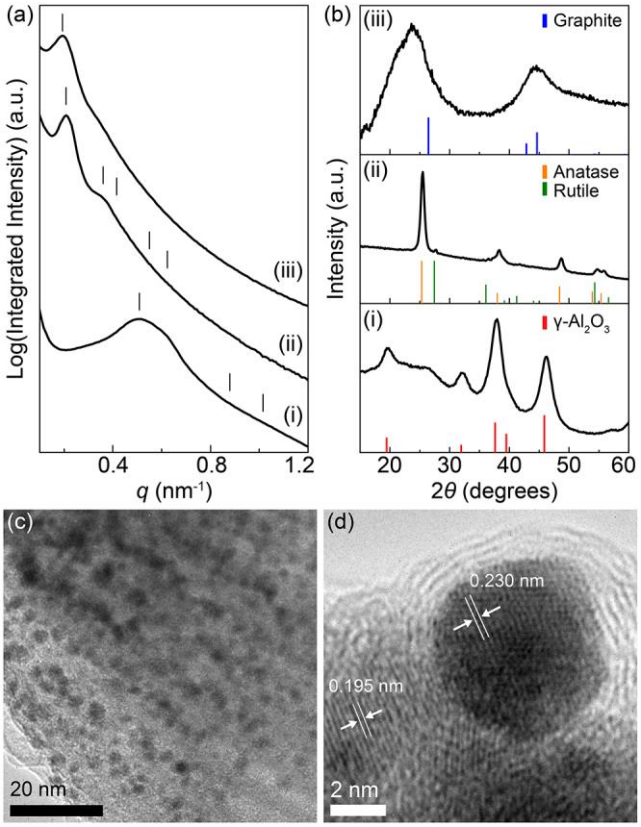

Figure 3. (a) SAXS and (b) WAXS data of SNAP composites: (i) Al_2O_3/MgO-C-100s, (ii) TiO_2-C-1s and (iii) carbon-50s. WAXS peak markings and relative intensities of γ-Al_2O_3 (red), anatase (orange, PDF 00-001-0562), rutile (green, PDF 04-003-0648) and graphite (blue, PDF 00-001-0646) are shown in (b). (c) TEM and (d) HR-TEM micrographs of Pt nanoparticles dispersed in γ-Al_2O_3-C-1s after Joule heating at 320 W.

SNAP is also suitable for all-organic BCP-directed hybrids such as PS-*b*-PEO-resols mesostructures. Both SAXS (Figure 3a) and TEM (Figure 2i) indicate retention of non-close-packed micellar structure with *d*-spacing of 32.6 nm after Joule heating at 300 W for 50 s. The broad (002) and (100) WAXS reflections of SNAP-carbon in Figure 3b centered at diffraction angles of 23.7° and 44.8°, indicate successful carbonization. Closer examination by HR-TEM (Figure 2i) reveals random clusters of graphitic sheets with moderately low crystallographic short-range order. This was corroborated by the Raman spectrum exhibiting strong intense D and G bands, as well as a relatively weak 2D band, centered at 1354, 1583

and 2876 cm^{-1}, respectively (Figure S8a).[32] Raman data analysis suggested an in-plane graphite cluster size (L_a) of ~3.7 nm (Figure S8b),[32,33] close to the crystallite size of ~2.8 nm from Scherrer analysis.

Rapid synthesis of ordered mesoporous inorganic supports with excellent thermal/chemical stability and pore connectivity coupled with catalytic metals can expand the functionality and application space. In a proof-of-principle experiment, chloroplatinic acid hexahydrate was impregnated into amorphous Al_2O_3-resin composite, followed by SNAP at 320 W for 1 s. Figure 3c and S9c shows the TEM image of platinum (Pt) nanoparticles with diameters of 2–20 nm aligned in the same direction as the SNAP-Al_2O_3-C hexagonal cylinders, corroborated by SAXS and WAXS (Figure S9a, b). HR-TEM in Figure 3d further reveals a 6-nm-diameter nanoparticle with lattice spacing of 0.230 nm matched with the (111) plane of face-centered cubic Pt, supported on a crystalline oxide-carbon framework with lattice spacing of 0.195 nm matched with the (400) plane of γ-Al_2O_3 (see also Figure S9d). The loading and distribution of catalytic metal nanoparticles in well-ordered mesoporous oxide-carbon structures could be improved, e.g., by adopting a "one-pot" synthesis approach that had demonstrated effective distribution of Pt-Pb nanoparticles in mesoporous niobium oxide-carbon structures for electrooxidation of formic acid.[9] Finally, this proof of concept here shows SNAP can enable simultaneous crystallization of multifunctional materials with ordered mesoporous architectures within seconds that may appeal to applications such as catalysis, carbon sequestration, energy storage and power generation.

ASSOCIATED CONTENT

Supporting Information

The Supporting Information is available free of charge at https://pubs.acs.org/doi/10.1021/

Experimental section and additional characterization data.

AUTHOR INFORMATION

Corresponding Author

Kwan W. Tan – E-mail: kwtan@ntu.edu.sg

Notes

H.G.O is a director of Smart Memories Pte Ltd. A provisional patent application related to this research has been filed by NTUitive Pte Ltd of Nanyang Technological University.

ACKNOWLEDGMENT

This work was supported by a member-directed research grant from ExxonMobil through the Singapore Energy Center (EM11161.TO6) and a startup grant from Nanyang Technological University, Singapore. This work made use of research facilities at the Facility for Analysis, Characterization, Testing and Simulation (FACTS), Nanyang Technological University, Singapore. We thank Y. Wu for kind experimental assistance and P. Buenconsejo and J. Lee for helpful discussion.

REFERENCES

(1) Kresge, C. T.; Leonowicz, M. E.; Roth, W. J.; Vartuli, J. C.; Beck, J. S. Ordered Mesoporous Molecular Sieves Synthesized by a Liquid-Crystal Template Mechanism. *Nature* **1992**, *359*, 710–712.

(2) Yang, P.; Zhao, D.; Margolese, D. I.; Chmelka, B. F.; Stucky, G. D. Generalized Syntheses of Large-Pore Mesoporous Metal Oxides with Semicrystalline Frameworks. *Nature* **1998**, *396*, 152–155.

(3) Joo, S. H.; Choi, S. J.; Oh, I.; Kwak, J.; Liu, Z.; Terasaki, O.; Ryoo, R. Ordered Nanoporous Arrays of Carbon Supporting High Dispersions of Platinum Nanoparticles. *Nature* **2001**, *412*, 169–172.

(4) Meng, Y.; Gu, D.; Zhang, F.; Shi, Y.; Yang, H.; Li, Z.; Yu, C.; Tu, B.; Zhao, D. Ordered Mesoporous Polymers and Homologous Carbon Frameworks: Amphiphilic Surfactant Templating and Direct Transformation. *Angew. Chem., Int. Ed.* **2005**, *44*, 7053–7059.

(5) Lee, J.; Orilall, M. C.; Warren, S. C.; Kamperman, M.; DiSalvo, F. J.; Wiesner, U. Direct Access to Thermally Stable and Highly Crystalline Mesoporous Transition-Metal Oxides with Uniform Pores. *Nat. Mater.* **2008**, *7*, 222–228.

(6) Werner, J. G.; Hoheisel, T. N.; Wiesner, U. Synthesis and Characterization of Gyroidal Mesoporous Carbons and Carbon Monoliths with Tunable Ultralarge Pore Size. *ACS Nano* **2014**, *8*, 731–743.

(7) Tan, K. W.; Sai, H.; Robbins, S. W.; Werner, J. G.; Hoheisel, T. N.; Hesse, S. A.; Beaucage, P. A.; DiSalvo, F. J.; Gruner, S. M.; Murtagh, M.; Wiesner, U. Ordered Mesoporous Crystalline Aluminas from Self-Assembly of ABC Triblock Terpolymer–Butanol–Alumina Sols. *RSC Adv.* **2015**, *5*, 49287–49294.

(8) Davis, M. E. Ordered Porous Materials for Emerging Applications. *Nature* **2002**, *417*, 813–821.

(9) Orilall, M. C.; Matsumoto, F.; Zhou, Q.; Sai, H.; Abruña, H. D.; DiSalvo, F. J.; Wiesner, U. One-Pot Synthesis of Platinum-Based Nanoparticles Incorporated into Mesoporous Niobium Oxide−Carbon Composites for Fuel Cell Electrodes. *J. Am. Chem. Soc.* **2009**, *131*, 9389–9395.

(10) Li, Y.; Horia, R.; Tan, W. X.; Larbaram, N.; Sasangka, W. A.; Manalastas, W.; Madhavi, S.; Tan, K. W. Mesoporous Titanium Oxynitride Monoliths from Block Copolymer-Directed Self-Assembly of Metal–Urea Additives. *Langmuir* **2020**, *36*, 10803–10810.

(11) Crossland, E. J. W.; Kamperman, M.; Nedelcu, M.; Ducati, C.; Wiesner, U.; Smilgies, D.-M.; Toombes, G. E. S.; Hillmyer, M. A.; Ludwigs, S.; Steiner, U.; Snaith, H. J. A Bicontinuous Double Gyroid Hybrid Solar Cell. *Nano Lett.* **2009**, *9*, 2807–2812.

(12) Tan, K. W.; Moore, D. T.; Saliba, M.; Sai, H.; Estroff, L. A.; Hanrath, T.; Snaith, H. J.; Wiesner, U. Thermally Induced Structural Evolution and Performance of Mesoporous Block Copolymer-Directed Alumina Perovskite Solar Cells. *ACS Nano* **2014**, *8*, 4730–4739.

(13) Werner, J. G.; Rodríguez-Calero, G. G.; Abruña, H. D.; Wiesner, U. Block Copolymer Derived 3-D Interpenetrating Multifunctional Gyroidal Nanohybrids for Electrical Energy Storage. *Energy Environ. Sci.* **2018**, *11*, 1261–1270.

(14) Hwang, J.; Jo, C.; Hur, K.; Lim, J.; Kim, S.; Lee, J. Direct Access to Hierarchically Porous Inorganic Oxide Materials with Three-Dimensionally Interconnected Networks. *J. Am. Chem. Soc.* **2014**, *136*, 16066–16072.

(15) Yuan, Q.; Yin, A.-X.; Luo, C.; Sun, L.-D.; Zhang, Y.-W.; Duan, W.-T.; Liu, H.-C.; Yan, C.-H. Facile Synthesis for Ordered Mesoporous γ-Aluminas with High Thermal Stability. *J. Am. Chem. Soc.* **2008**, *130*, 3465–3472.
(16) Seah, G. L.; Wang, L.; Tan, L. F.; Tipjanrawee, C.; Sasangka, W. A.; Usadi, A. K.; McConnachie, J. M.; Tan, K. W. Formation Pathways of Highly Ordered Alumina Mesostructures with Tunable Morphologies and Pore Sizes. **2021**.
(17) Zhu, Y.; Zhao, Y.; Ma, J.; Cheng, X.; Xie, J.; Xu, P.; Liu, H.; Liu, H.; Zhang, H.; Wu, M.; Elzatahry, A. A.; Alghamdi, A.; Deng, Y.; Zhao, D. Mesoporous Tungsten Oxides with Crystalline Framework for Highly Sensitive and Selective Detection of Foodborne Pathogens. *J. Am. Chem. Soc.* **2017**, *139*, 10365–10373.
(18) Ren, Y.; Zou, Y.; Liu, Y.; Zhou, X.; Ma, J.; Zhao, D.; Wei, G.; Ai, Y.; Xi, S.; Deng, Y. Synthesis of Orthogonally Assembled 3D Cross-Stacked Metal Oxide Semiconducting Nanowires. *Nat. Mater.* **2020**, *19*, 203–211.
(19) Robbins, S. W.; Beaucage, P. A.; Sai, H.; Tan, K. W.; Werner, J. G.; Sethna, J. P.; DiSalvo, F. J.; Gruner, S. M.; Dover, R. B. V.; Wiesner, U. Block Copolymer Self-Assembly–Directed Synthesis of Mesoporous Gyroidal Superconductors. *Sci. Adv.* **2016**, *2*, e1501119.
(20) Tan, K. W.; Wiesner, U. Block Copolymer Self-Assembly Directed Hierarchically Structured Materials from Nonequilibrium Transient Laser Heating. *Macromolecules* **2019**, *52*, 395–409.
(21) Tan, K. W.; Jung, B.; Werner, J. G.; Rhoades, E. R.; Thompson, M. O.; Wiesner, U. Transient Laser Heating Induced Hierarchical Porous Structures from Block Copolymer–Directed Self-Assembly. *Science* **2015**, *349*, 54–58.
(22) Tan, K. W.; Werner, J. G.; Goodman, M. D.; Kim, H. S.; Jung, B.; Sai, H.; Braun, P. V.; Thompson, M. O.; Wiesner, U. Synthesis and Formation Mechanism of All-Organic Block Copolymer-Directed Templating of Laser-Induced Crystalline Silicon Nanostructures. *ACS Appl. Mater. Interfaces* **2018**, *10*, 42777–42785.
(23) Yu, F.; Zhang, Q.; Thedford, R. P.; Singer, A.; Smilgies, D.-M.; Thompson, M. O.; Wiesner, U. B. Block Copolymer Self-Assembly-Directed and Transient Laser Heating-Enabled Nanostructures toward Phononic and Photonic Quantum Materials. *ACS Nano* **2020**, *14*, 11273–11282.
(24) Arora, H.; Du, P.; Tan, K. W.; Hyun, J. K.; Grazul, J.; Xin, H. L.; Muller, D. A.; Thompson, M. O.; Wiesner, U. Block Copolymer Self-Assembly–Directed Single-Crystal Homo- and Heteroepitaxial Nanostructures. *Science* **2010**, *330*, 214–219.
(25) Zhang, Y.; Bhaway, S. M.; Wang, Y.; Cavicchi, K. A.; Becker, M. L.; Vogt, B. D. Rapid (<3 Min) Microwave Synthesis of Block Copolymer Templated Ordered Mesoporous Metal Oxide and Carbonate Films Using Nitrate–Citric Acid Systems. *Chem. Commun.* **2015**, *51*, 4997–5000.
(26) Yao, Y.; Huang, Z.; Xie, P.; Lacey, S. D.; Jacob, R. J.; Xie, H.; Chen, F.; Nie, A.; Pu, T.; Rehwoldt, M.; Yu, D.; Zachariah, M. R.; Wang, C.; Shahbazian-Yassar, R.; Li, J.; Hu, L. Carbothermal Shock Synthesis of High-Entropy-Alloy Nanoparticles. *Science* **2018**, *359*, 1489–1494.
(27) Lacey, S. D.; Dong, Q.; Huang, Z.; Luo, J.; Xie, H.; Lin, Z.; Kirsch, D. J.; Vattipalli, V.; Povinelli, C.; Fan, W.; Shahbazian-Yassar, R.; Wang, D.; Hu, L. Stable Multimetallic Nanoparticles for Oxygen Electrocatalysis. *Nano Lett.* **2019**, *19*, 5149–5158.
(28) Wang, C.; Ping, W.; Bai, Q.; Cui, H.; Hensleigh, R.; Wang, R.; Brozena, A. H.; Xu, Z.; Dai, J.; Pei, Y.; Zheng, C.; Pastel, G.; Gao, J.; Wang, X.; Wang, H.; Zhao, J.-C.; Yang,

B.; Zheng, X. (Rayne); Luo, J.; Mo, Y.; Dunn, B.; Hu, L. A General Method to Synthesize and Sinter Bulk Ceramics in Seconds. *Science* **2020**, *368*, 521–526.
(29) Luong, D. X.; Bets, K. V.; Algozeeb, W. A.; Stanford, M. G.; Kittrell, C.; Chen, W.; Salvatierra, R. V.; Ren, M.; McHugh, E. A.; Advincula, P. A.; Wang, Z.; Bhatt, M.; Guo, H.; Mancevski, V.; Shahsavari, R.; Yakobson, B. I.; Tour, J. M. Gram-Scale Bottom-up Flash Graphene Synthesis. *Nature* **2020**, *577*, 647–651.
(30) Morris, S. M.; Fulvio, P. F.; Jaroniec, M. Ordered Mesoporous Alumina-Supported Metal Oxides. *J. Am. Chem. Soc.* **2008**, *130*, 15210–15216.
(31) Gajjela, S. R.; Ananthanarayanan, K.; Yap, C.; Grätzel, M.; Balaya, P. Synthesis of Mesoporous Titanium Dioxide by Soft Template Based Approach: Characterization and Application in Dye-Sensitized Solar Cells. *Energy Environ. Sci.* **2010**, *3*, 838–845.
(32) Ferrari, A. C.; Robertson, J. Interpretation of Raman Spectra of Disordered and Amorphous Carbon. *Phys. Rev. B* **2000**, *61*, 14095–14107.
(33) Cançado, L. G.; Takai, K.; Enoki, T.; Endo, M.; Kim, Y. A.; Mizusaki, H.; Jorio, A.; Coelho, L. N.; Magalhães-Paniago, R.; Pimenta, M. A. General Equation for the Determination of the Crystallite Size La of Nanographite by Raman Spectroscopy. *Appl. Phys. Lett.* **2006**, *88*, 163106.

EXPERIMENTAL SECTION

Materials. All chemicals were used as received. Pluronic F127 (PEO-*b*-PPO-*b*-PEO, 12.6 kg/mol), aluminum tri-*sec*-butoxide ($Al(O^sBu)_3$), 97%), magnesium nitrate hexahydrate ($Mg(NO_3)_2{\cdot}6H_2O$, ACS reagent, 99%), titanium isopropoxide (≥97%), chloroplatinic acid hexahydrate ($H_2PtCl_6{\cdot}6H_2O$, ACS reagent, 37.5% Pt basis) and tetrahydrofuran (anhydrous, inhibitor-free) were obtained from Sigma-Aldrich. Absolute ethanol (EtOH, 200 proof) was obtained from Merck. Nitric acid (HNO_3, 69 wt%) and hydrochloric acid (HCl, 37%) was obtained from Honeywell International. The carbon paper was obtained from Fuel Cell Earth.

Synthesis of F127–Al_2O_3 Hybrid Monoliths. 3.76 g (81.7 mmol) of EtOH was added to 1 g (4.0 mmol) of $Al(O^sBu)_3$ and left undisturbed for 30 min, followed by vigorous stirring for another 30 min, forming a white cloudy suspension due to alcoholysis. 0.421 mL (6.5 mmol) of HNO_3 was carefully added into the cloudy mixture and stirred vigorously for 12 h to obtain a colorless transparent Al_2O_3 sol solution under ambient conditions. 1.53 g aliquot (18.7 wt% $Al(O^sBu)_3$) was then added into 1.80 g F127 solution (10 wt% in EtOH) and stirred for 30 min. The colorless transparent hybrid solution was cast in 5 mL PTFE beakers set on a glass Petri dish covered with hemispherical glass dome and heated at 50 °C for evaporation-induced self-assembly (EISA) over 3–7 days under ambient conditions. The hybrid monolithic samples were cured in a vacuum oven at 25 °C (20 min), 40 °C (50 min), 60 °C (>12 h), 100 °C (2 h) and finally 130 °C (2h).

Synthesis of F127–Al_2O_3/MgO Hybrid Monoliths. 3.76 g (81.7 mmol) of EtOH was added to 0.9 g (3.6 mmol) $Al(O^sBu)_3$ and left undisturbed for 30 min, followed by vigorous stirring for another 30 min. 0.368 mL (5.7 mmol) HNO_3 was then added into the white cloudy mixture and stirred 24 h to obtain a transparent Al_2O_3 sol solution. 0.12 g (0.4 mmol) of $Mg(NO_3)_2{\cdot}6H_2O$ was added into the Al_2O_3 sol and stirred thoroughly for 1 h to fully dissolve the Mg nitrate salt. 1.53 g aliquot of the resultant Al_2O_3/MgO sol solution was added into 1.80 g of 10 wt% F127 solution, followed by EISA and thermal curing as described above.

Synthesis of PS-*b*-PEO–TiO_2 and PS-*b*-PEO–Resols Hybrid Monoliths. A linear polystyrene-block-polyethylene oxide (PS-*b*-PEO) block copolymer with molar mass of 47.4 kg/mol, polydispersity index of 1.2, composition of 89.5 wt% PS and 10.5 wt% PEO, was synthesized by atomic-transfer racial polymerization (ATRP) as reported elsewhere.[1] The synthesis of phenol-formadelyde resols in tetrahydrofuran (20 wt%) was prepared as reported elsewhere.[2]

The PS-*b*-PEO–TiO_2 hybrid monolith samples were prepared as reported elsewhere.[3] Briefly, 0.1 g of PS-*b*-PEO was first dissolved in 2 mL tetrahydrofuran. In a separate vial, 0.64 mL of HCl (37%) was added into 2 mL of titanium isopropoxide, and stirred vigorously for 5 min, followed by addition of 5 mL of tetrahydrofuran and stirred for another 2 min. 1.5 mL aliquot of the transparent yellow-colored TiO_2 sol solution was added into PS-*b*-PEO solution and stirred for 30 min, followed by EISA at 50 °C (>36 h) and thermal curing at 130 °C in a

vacuum oven overnight.

For the all-organic PS-*b*-PEO-resols monoliths, 1.15 g aliquot of 20 wt% resols was mixed in 1 g of PS-*b*-PEO solution (10 wt% in tetrahydrofuran) and stirred for 24 hours, followed by EISA at 50 °C (>24 h) and then thermal curing at 100 °C in a vacuum oven overnight.

Thermopolymerization of F127–Al_2O_3, F127–Al_2O_3/MgO, PS-*b*-PEO–TiO_2 and PS-*b*-PEO–Resols Monoliths. The F127–Al_2O_3 and F127–Al_2O_3/MgO hybrids were heated in a tube furnace at 400 °C (2 h) with a ramp rate of 1 °C/min under nitrogen to thermopolymerize the BCP into resin. The PS-*b*-PEO–resols hybrids were heated at 300 °C (1.5 h) with ramp rate of 1 °C/min under nitrogen to thermopolymerize the BCP and resols additive into resin. The PS-*b*-PEO–TiO_2 hybrids were cured in a vacuum oven at 200 °C (1 h) to form the TiO_2-resin composite.

Joule heating of ordered mesoporous Al_2O_3, Al_2O_3-MgO, TiO_2 and resin monoliths. The Joule heating experiments were performed with a home-built setup as described in previous literature.[4,5] Briefly, the monolithic samples were inserted between two parallel carbon papers (4-cm-length and 1-cm-width) that were suspended in a 2-inch quartz tube under mild vacuum (<1 torr). A MAISHENG source meter was used to supply tunable current and potential values up to 20 A and 30 V, respectively. The hybrid monolith samples were heated at powers of 70 to 420 W with a ramp dwell of 3 s and holding dwells of 1 to 100 s. ***CAUTION!*** There are serious risks of electrical shock or even electrocution. Electrical safety measures described in ref. 5 were implemented for all users.

Synthesis of crystalline mesoporous SNAP-all-oxide structures. The Al_2O_3-hybrid was heated in a tube furnace under static air at 450 °C (3 h) with a ramp rate of 1 °C/min. The amorphous Al_2O_3 monolith was then Joule-heated at 360 W for 5 s as described above, yielding the resultant mesoporous all-γ-Al_2O_3.

The cured TiO_2-resin monolith was Joule-heated at 240 W for 1 s as described above. The resultant anatase-TiO_2-C composite was then heated in a box furnace under static air at 400 °C (0.5 h) with a ramp rate of 1 °C/min, yielding the resultant mesoporous all-anatase-TiO_2.

Impregnation of chloroplatinic acid in mesoporous Al_2O_3-resin structures. 0.1 g of thermally cured Al_2O_3-resin added into a round bottom flask and degassed overnight under vacuum at room temperature. 2 mL of 0.01 M $H_2PtCl_6{\cdot}6H_2O$ dissolved in ethanol was gradually added on the composite monolith. The H_2PtCl_6-impregnated Al_2O_3-resin composite was left under ambient conditions for 12 h, and then placed in a vacuum oven at 60 °C for another 2 h. The H_2PtCl_6-impregnated Al_2O_3-resin was Joule-heated at 320 W for 1 s as described above.

Characterization. Small- and wide-angle X-ray scattering (SAXS/WAXS) measurements were collected with a Xenocs Nano-inXider using Cu K_α radiation source and Dectris Pilatus 3 detectors. 2D SAXS/WAXS patterns were azimuthally integrated around the beam center into 1D scattering intensity curves plotted against the scattering vector magnitude $q = 4\pi \sin\theta/\lambda$, where θ is half of the total scattering angle and λ is the X-ray wavelength. The cylinder-to-cylinder *d*-spacing of *p6mm* lattice was calculated using $d = 4\pi/(\sqrt{3}q^*)$, where q^* is the scattering vector of the principal peak. The *d*-spacing of non-close-packed micellar lattice was calculated using $d = 2\pi/q^*$.

Transmission electron micrographs (TEM) were obtained using the JEOL 2010 and 2100F electron microscopes operating at the accelerating voltage of 200 kV equipped with the AMT XR40B CCD camera and Gatan Ultrascan 1000XP CCD camera, respectively. Energy-dispersive spectroscopy was performed using the JEOL 2100F equipped with an EDAX EDS detector at 200 kV.

Thermogravimetric analysis (TGA) measurements were conducted using a TA Instruments Q500 in air with a heating rate of 10 °C/min.

Raman spectroscopy measurements were conducted using a WITec Alpha300 SR with a 488 nm excitation laser source. The in-plane graphite cluster size was calculated using the equation $L_a\ (nm) = (2.4 \times 10^{-10})\lambda_l^4 (I_D/I_G)^{-1}$, where λ_l is the excitation laser wavelength and (I_D/I_G) is the integrated intensity ratio of the D and G bands fitted to the Lorentzian and Breit-Wigner-Fano (BWF) functions, respectively.[2,6]

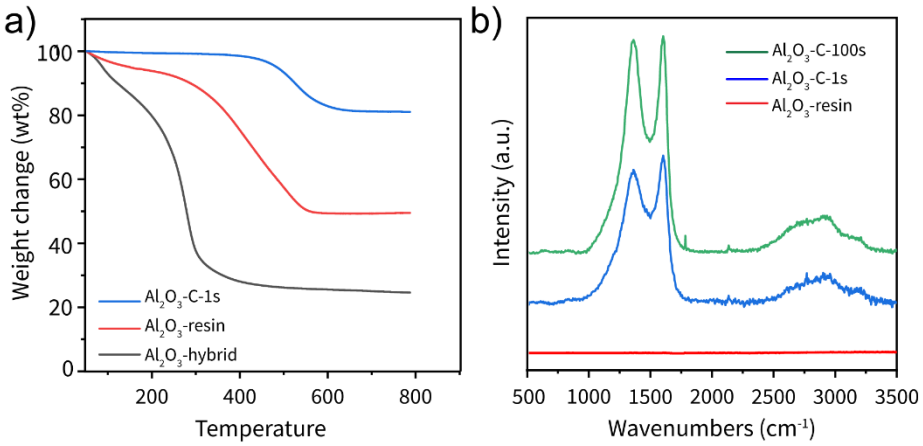

Figure S1. (a) TGA data for SNAP-Al_2O_3 samples: as-made Al_2O_3-hybrid (black curve), Al_2O_3-resin after thermal curing (red curve), and Al_2O_3-C-1s composite after Joule heating at 360 W for 1 s (blue curve). The organic content was reduced from 76 wt % to 50 wt% after thermopolymerization. The resultant Al_2O_3-C-1s was composed of 19 wt% carbon and 81 wt% Al_2O_3 after Joule heating. (b) Raman spectra (488 nm excitation) of SNAP-Al_2O_3 samples. The absence of D- and G-bands in the Al_2O_3-resin (red curve) confirms the organic nature of thermopolymerized resin matrix after thermal curing. The appearance and increasing intensities of the D-, G- and 2D-bands for Al_2O_3-C-1s (blue curve) and Al_2O_3-C-100s (green curve) after Joule heating at 360 W for 1 and 100 s, respectively, indicate conversion of resin matrix into carbon.

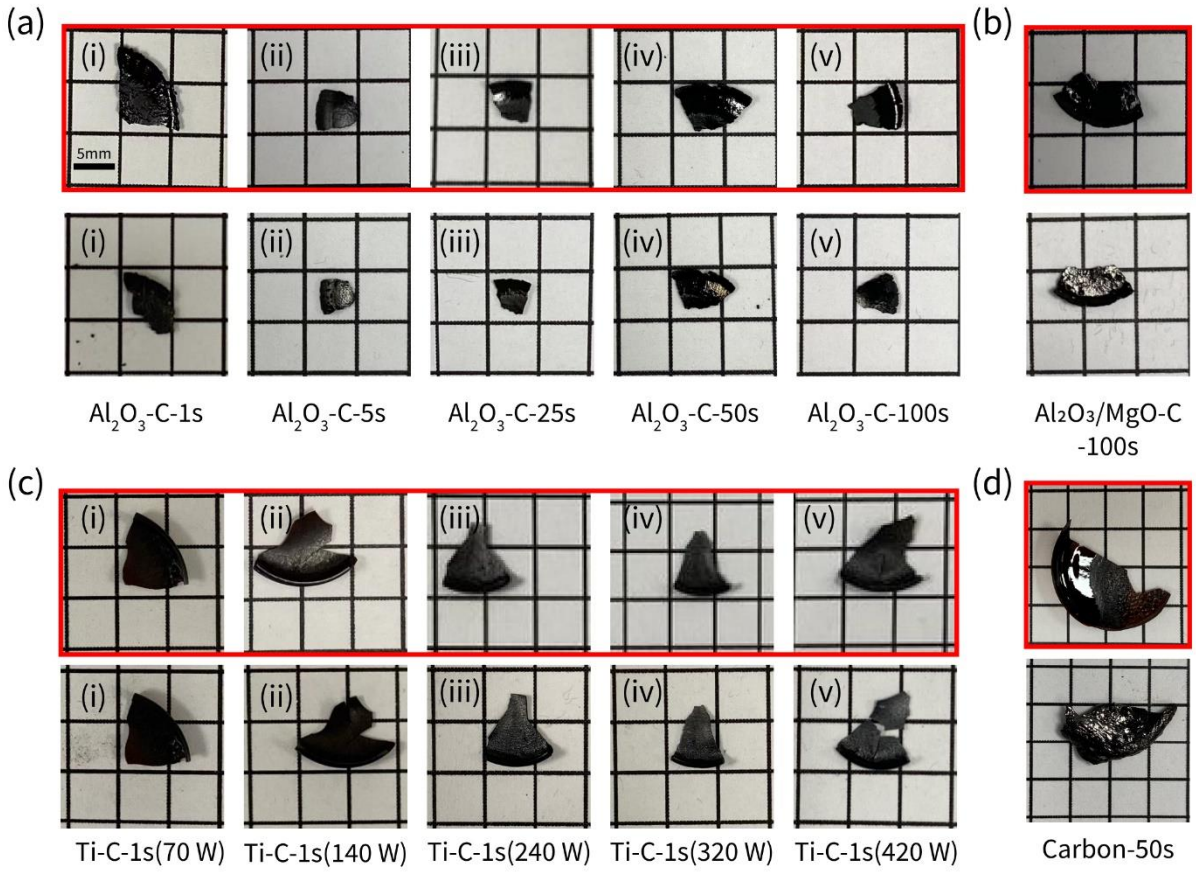

Figure S2. Optical images of monolithic samples of block copolymer-directed composites, before (highlighted in the red-colored boxes) and after Joule heating, as indicated: (a) SNAP-Al_2O_3, (b) SNAP-Al_2O_3/MgO, (c) SNAP-TiO_2 and (d) SNAP-carbon. The macroscopic shape and integrity of all samples were retained after Joule heating despite thermal shrinkage. The grid papers have 5-mm markings.

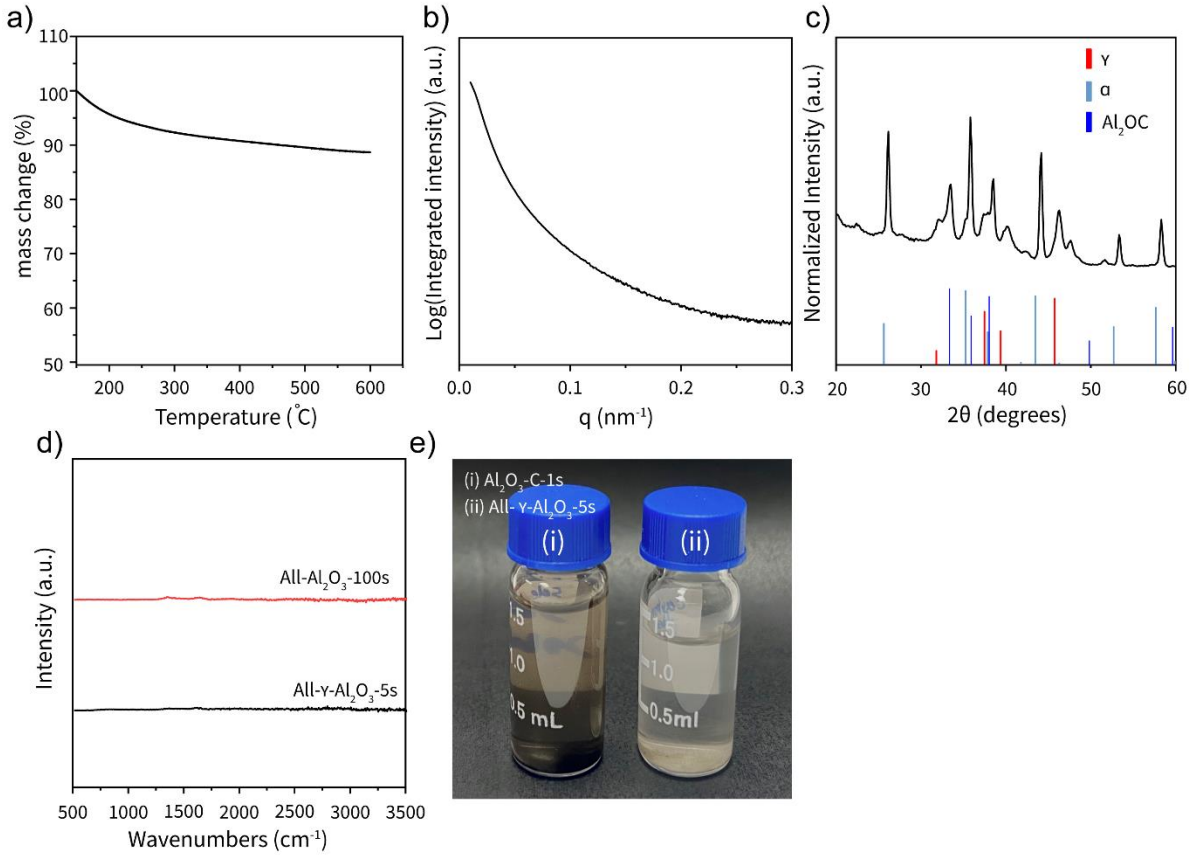

Figure S3. (a) TGA data of the amorphous Al_2O_3 after calcination in air at 450°C for 3 h, indicating the sample is mostly inorganic (~90 wt%). (b) SAXS and (c) WAXS patterns of Al_2O_3-100s sample that was Joule-heated at 360 W for 100 s. SAXS implies the sample mesostructure completely collapsed. WAXS attributes the mesostructure collapse to the extensive crystallite growth of α-Al_2O_3 (blue, PDF 04-004-2852) and aluminum oxycarbide (Al_2OC, dark blue, PDF 01-072-3584). It should be noted that WAXS reflections suggest presence of other crystalline Al_2O_3-based compounds that were most likely formed through reactions with the carbon paper. (d) Raman spectra of the all-Al_2O_3 samples annealed at 360 W for 5 s (black curve) and 100 s (red curve) as indicated. The black-colored Raman spectrum is flat indicating absence of carbon matrix in the samples. (e) Optical image of SNAP-Al_2O_3 powdered samples dispersed in ethanol for TEM sample preparation. The Al_2O_3-C-1s suspension appears brownish black attributed to the presence of carbon matrix, whereas the all-γ-Al_2O_3-5s suspension appears pale white indicating absence of carbon, consistent with TGA and Raman spectroscopy.

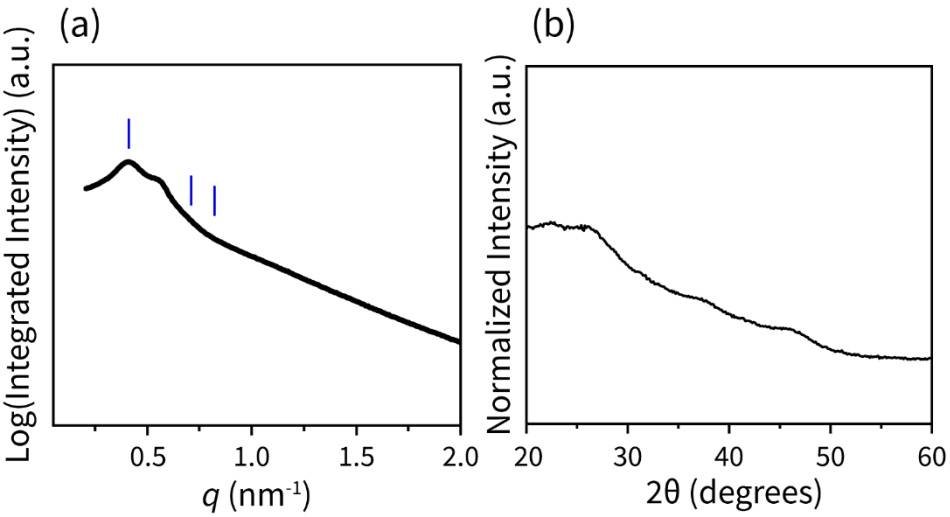

Figure S4. (a) SAXS pattern of Al_2O_3/MgO-C-1s after Joule heating at 300 W for 1 s. The blue-colored tick marks indicate the expected SAXS reflections for *p6mm* lattice. The shoulder on the right-hand-side of the primary peak suggests the sample may have a second mesophase. (b) The absence of peaks in the WAXS pattern of Al_2O_3/MgO-C-1s indicates SNAP duration of 1 s at 360 W was insufficient to induce crystallization.

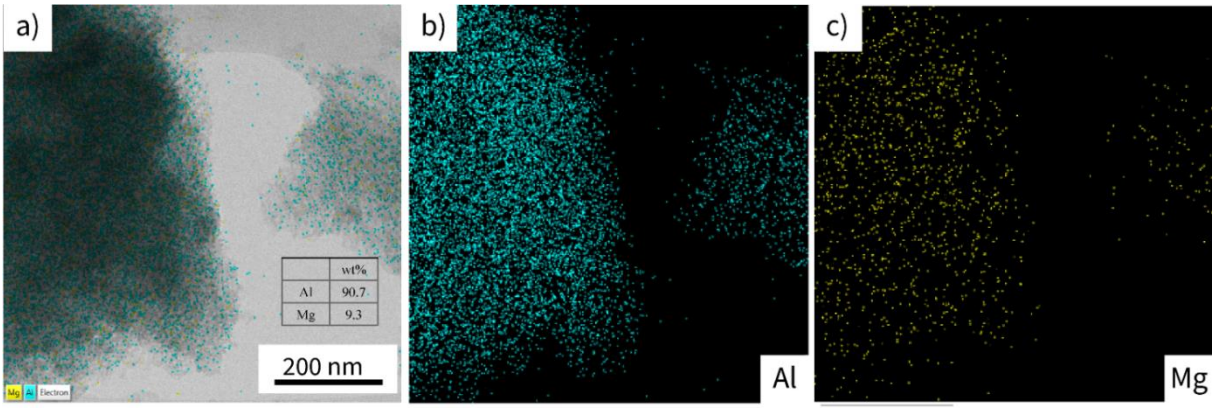

Figure S5. (a) Electron dispersive spectroscopy elemental mapping of Al_2O_3/MgO-C-100s shows homogeneous distribution of (b) Al and (c) Mg in the ordered mesostructure. EDS indicates 90.7 wt% Al and 9.3 wt% Mg in the sample, that is almost identical to the mass ratio of Al/Mg = 9:1 in the mixed oxide sol precursors.

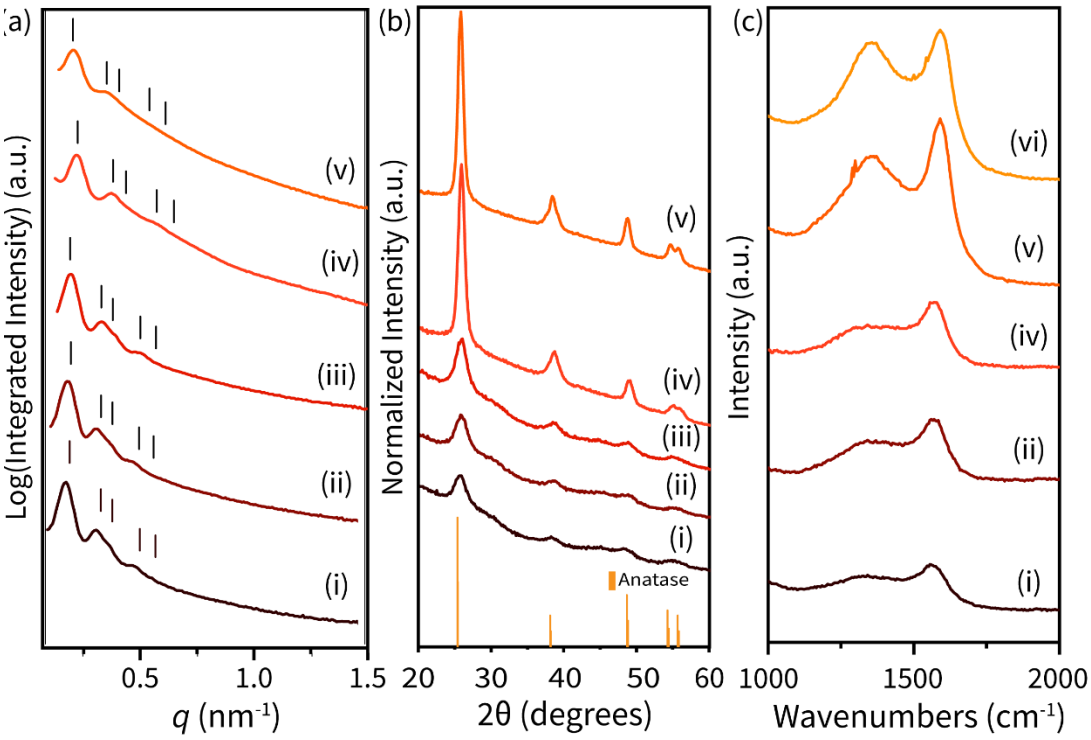

Figure S6. (a) SAXS, (b) WAXS and (c) Raman spectra (488 nm excitation) of SNAP-TiO_2 composite samples: (i) TiO_2-resin after curing at 200 °C, (ii) TiO_2-C-1s(70 W), (iii) TiO_2-C-1s(140 W), (iv) TiO_2-C-1s(240 W), (v) TiO_2-C-1s(320 W), and (vi) TiO_2-C-1s(420 W). Tick marks in (a) indicate the expected SAXS reflections for *p6mm* lattice. WAXS peak markings and relative intensities are shown for anatase TiO_2 (PDF 00-001-0562) in (b). (a) SAXS patterns indicate the *p6mm* symmetry is preserved for all the SNAP-TiO_2-C composites after Joule heating with increasing powers up to 320 W. (b) The increased intensities and reduced full-width-half-maximum values of the WAXS reflections indicate improved anatase TiO_2 crystallinity as the input power increased from 70 to 320 W. (c) The augmented intensities of the D- and G-bands in the Raman spectra imply higher input powers promote graphitization of the carbon matrices.

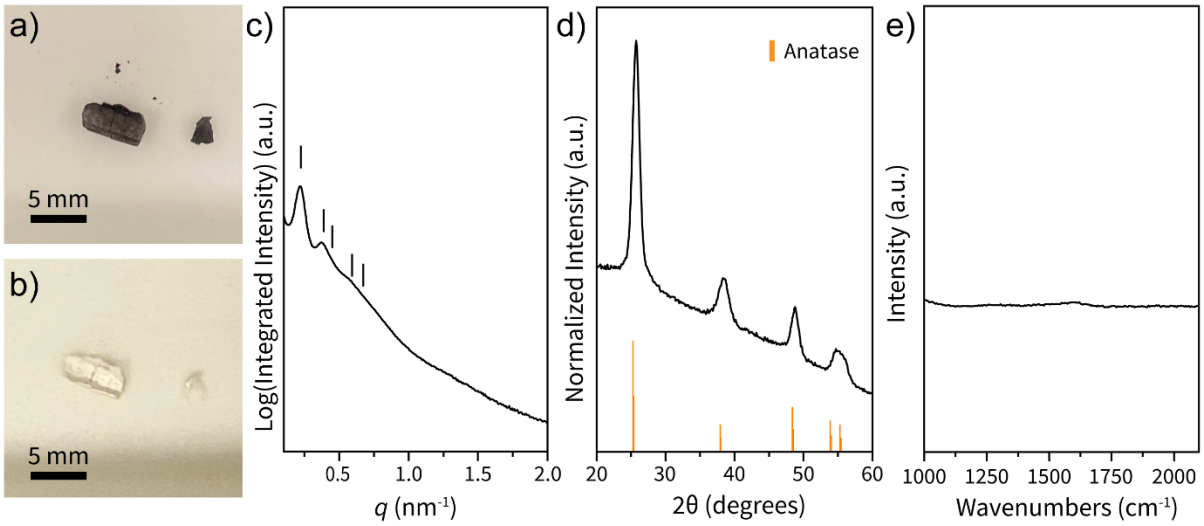

Figure S7. (a, b) Optical images of (a) black-colored TiO_2-C-1s(240 W) composite after Joule heating and (b) white-colored all-anatase-TiO_2-1s(240 W) after removing the carbon at 400 °C in air for 30 min. (c) SAXS and (d) WAXS patterns of mesoporous all-anatase-TiO_2-1s(240 W) indicating preservation of the *p6mm* symmetry and anatase TiO_2 crystallites, respectively, after carbon removal. (e) The absence of D- and G-bands in the Raman spectrum (488 nm excitation) of all-anatase-TiO_2-1s(240 W) confirms complete carbon removal.

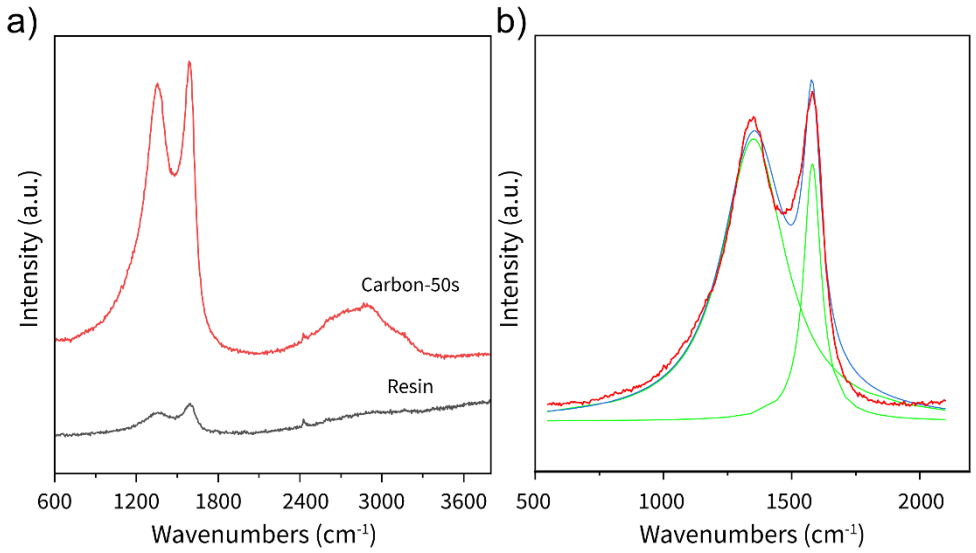

Figure S8. (a) Raman spectra (488 nm excitation) of thermally cured PS-*b*-PEO-resin (black curve) and SNAP-carbon-50s after Joule heating at 300 W for 50 s (red curve). The appearance of strong intense D- and G-bands as well as a broad 2D-band indicates conversion of phenolic resin into carbon. (b) The Raman spectra of SNAP-carbon-50s was fitted between 550 and 2100 cm^{-1} using the Lorentzian and Breit-Wigner-Fano (BWF) functions for the D- and G-band, respectively, giving an integrated intensity ratio (I_D/I_G) of 3.6.

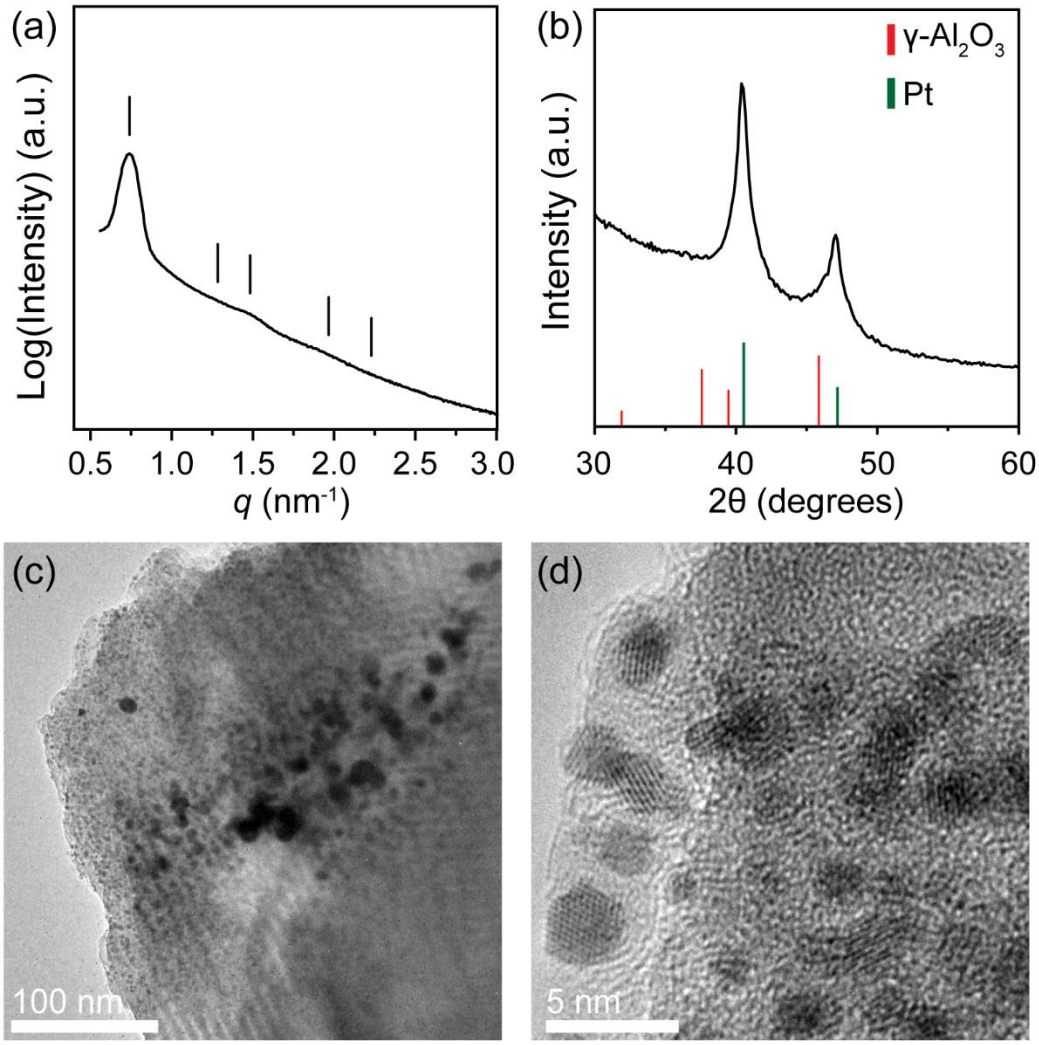

Figure S9. (a) SAXS and (b) WAXS patterns of Pt/γ-Al_2O_3-C-1s composite after Joule heating at 320 W for 1 s, confirming preservation of *p6mm* morphology and simultaneous crystallization of Pt nanoparticles on mesoporous γ-Al_2O_3-carbon support. WAXS peak markings and relative intensities are shown for γ-Al_2O_3 (red, PDF 00-010-0425) and Pt (green, PDF 01-085-5658) in (b). The two sharp peaks at diffraction angles of 40.6° and 47.2° were indexed to the (111) and (200) planes of Pt, while the broad shoulder at 46.0° was indexed to the (400) plane of γ-Al_2O_3. (c) A lower magnification TEM image of Pt/γ-Al_2O_3-C-1s composite. (d) HR-TEM micrograph of Pt nanoparticles on the γ-Al_2O_3-carbon composite.

REFERENCES

(1) Hwang, J.; Jo, C.; Hur, K.; Lim, J.; Kim, S.; Lee, J. Direct Access to Hierarchically Porous Inorganic Oxide Materials with Three-Dimensionally Interconnected Networks. *J. Am. Chem. Soc.* **2014**, *136*, 16066–16072.

(2) Werner, J. G.; Hoheisel, T. N.; Wiesner, U. Synthesis and Characterization of Gyroidal Mesoporous Carbons and Carbon Monoliths with Tunable Ultralarge Pore Size. *ACS Nano* **2014**, *8*, 731–743.

(3) Tan, K. W.; Moore, D. T.; Saliba, M.; Sai, H.; Estroff, L. A.; Hanrath, T.; Snaith, H. J.; Wiesner, U. Thermally Induced Structural Evolution and Performance of Mesoporous Block Copolymer-Directed Alumina Perovskite Solar Cells. *ACS Nano* **2014**, *8*, 4730–4739.

(4) Wang, C.; Ping, W.; Bai, Q.; Cui, H.; Hensleigh, R.; Wang, R.; Brozena, A. H.; Xu, Z.; Dai, J.; Pei, Y.; Zheng, C.; Pastel, G.; Gao, J.; Wang, X.; Wang, H.; Zhao, J.-C.; Yang, B.; Zheng, X. (Rayne); Luo, J.; Mo, Y.; Dunn, B.; Hu, L. A General Method to Synthesize and Sinter Bulk Ceramics in Seconds. *Science* **2020**, *368*, 521–526.

(5) Luong, D. X.; Bets, K. V.; Algozeeb, W. A.; Stanford, M. G.; Kittrell, C.; Chen, W.; Salvatierra, R. V.; Ren, M.; McHugh, E. A.; Advincula, P. A.; Wang, Z.; Bhatt, M.; Guo, H.; Mancevski, V.; Shahsavari, R.; Yakobson, B. I.; Tour, J. M. Gram-Scale Bottom-up Flash Graphene Synthesis. *Nature* **2020**, *577*, 647–651.

(6) Cançado, L. G.; Takai, K.; Enoki, T.; Endo, M.; Kim, Y. A.; Mizusaki, H.; Jorio, A.; Coelho, L. N.; Magalhães-Paniago, R.; Pimenta, M. A. General Equation for the Determination of the Crystallite Size La of Nanographite by Raman Spectroscopy. *Appl. Phys. Lett.* **2006**, *88*, 163106.